Biosolar Oxygenation of Hydrocarbons by Photocatalytic Artificial Wood

Jang, Jinha; Aurangzeb Khan, Waseela; Hollmann, Frank; Won, Keehoon; Park, Chan Beum

DOI
10.1021/acssuschemeng.4c02882

Publication date
2024

Document Version
Final published version

Published in
ACS Sustainable Chemistry and Engineering

ACS Sustainable Chemistry & Engineering

pubs.acs.org/journal/ascecg

Research Article

Biosolar Oxygenation of Hydrocarbons by Photocatalytic Artificial Wood

Jinha Jang, Waseela Aurangzeb Khan, Frank Hollmann, Keehoon Won,* and Chan Beum Park*

Cite This: *ACS Sustainable Chem. Eng.* 2024, 12, 8950−8957

Read Online

ACCESS | Metrics & More | Article Recommendations | Supporting Information

ABSTRACT: Lignin is the most abundant renewable and sustainable source of aromatic compounds to replace fossil resources, causing environmental issues. However, most lignin generated from pulping and biorefinery processes is combusted or discarded as waste. In this work, we first propose a photocatalytic artificial wood platform consisting of lignin and cellulose, inspired by woody cell walls, where lignin is arranged around cellulose fibers. The wood-mimetic particles were fabricated through reconstitution after the complete dissolution of lignin and cellulose. Intensive characterization revealed that the introduction of cellulose suppressed lignin's self-aggregation, which limits its practical photocatalytic applications. As a result, the artificial wood photocatalyst exhibited a 3.2 times higher production rate of H_2O_2 from oxygen and water than lignin under solar light. The wood-mimetic photocatalyst was further coupled with an unspecific peroxygenase (UPO) biocatalyst to catalyze the selective oxygenation of inert C−H bonds using H_2O_2 as an oxidant. The wood-UPO hybrid catalyst demonstrated a universal photobiocatalytic oxyfunctionalization of various hydrocarbons with a higher total turnover number and turnover frequency than the lignin-UPO catalyst. This work suggests a practical strategy to utilize waste lignin as a photocatalyst and further demonstrates sustainable biosolar oxygenation reactions using sunlight and water as green energy and electron sources, respectively.

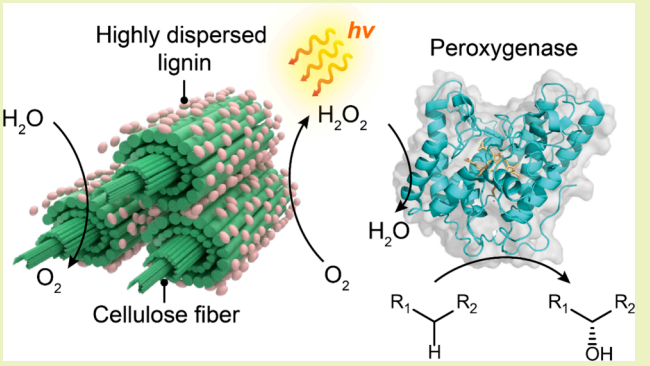

KEYWORDS: *artificial wood, lignin, cellulose, aggregation, oxyfunctionalization, oxygen photoreduction, photobiocatalysis*

INTRODUCTION

Lignin is a complex aromatic polymer comprising the cells of most plants, which accounts for about 15−30% of the solid weight of plants. Its structure is a random network of monomeric phenylpropanes such as *p*-hydroxyphenyl (H), guaiacyl (G), and syringyl (S) units, which are derived from the monolignols of *p*-coumaryl-, coniferyl-, and sinapyl alcohol, respectively. It is a promising renewable and sustainable resource to replace fossil resources, which cause global warming and environmental pollution. Despite its potential, approximately 50 million metric tons of lignin generated from pulping and biorefinery processes is mostly combusted or discarded due to its complex and heterogeneous structure. Over the last two decades, the research on lignin valorization has evolved, focusing on the development of lignin-derived chemicals and materials for various applications.[1−3] Moving beyond the conventional approaches to lignin utilization, our group has recently revealed that lignin functions as a photocatalyst for hydrogen peroxide generation from oxygen enabled by its exceptional light absorption, charge separation, and charge transfer capabilities.[4] Lignin generates H_2O_2 via a β-O-4-mediated O_2 reduction using water as an electron donor upon photosensitization of aromatic groups such as G and H units.

In general, molecules form self-aggregates by various intermolecular interactions, which can significantly decrease the activity of molecular catalysts in reaction media.[5−9] Aggregation decreased the photocatalytic efficiency of flavins by quenching excited states or by altering their redox properties.[5] Upon self-association in solution, the photocatalytic activity of phthalocyanine complexes decreased by 5 to 10 times because the excited state was quenched.[6] The increase in the concentration of cobalt porphyrin decreased the catalytic activity due to aggregation to lower the percentage of active molecules available for catalysis, and catalyst aggregation dictated the quantity of active species.[7] Lignin aggregates in both aqueous and organic solvents mainly by intermolecular $\pi-\pi$ interactions and hydrogen bonding.[10,11] Lignin's inclina-

Received: April 6, 2024
Revised: May 18, 2024
Accepted: May 20, 2024
Published: May 31, 2024

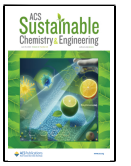

tion to form aggregates should limit its practical photocatalytic applications, particularly at high concentrations, because such aggregates screen the redox moiety (e.g., C_α−OH in the β-O-4 linkage) of lignin, decreasing the efficiency of the photoreduction of O_2 to H_2O_2.

As an integral part of woody cell walls, lignin exists in a homogeneous space arrangement around cellulose strands.[12,13] This natural structure inspired us to address the lignin aggregation problem. Herein, for the first time, we suggest artificial wood consisting of lignin and cellulose as a high-efficiency photocatalyst without aggregation, as depicted in Scheme 1. The wood-mimetic powder is easily prepared by the

Scheme 1. Schematic of Photobiocatalytic Oxyfunctionalization with Peroxygenase and Artificial Wood Consisting of Lignin and Cellulose Fibers[a]

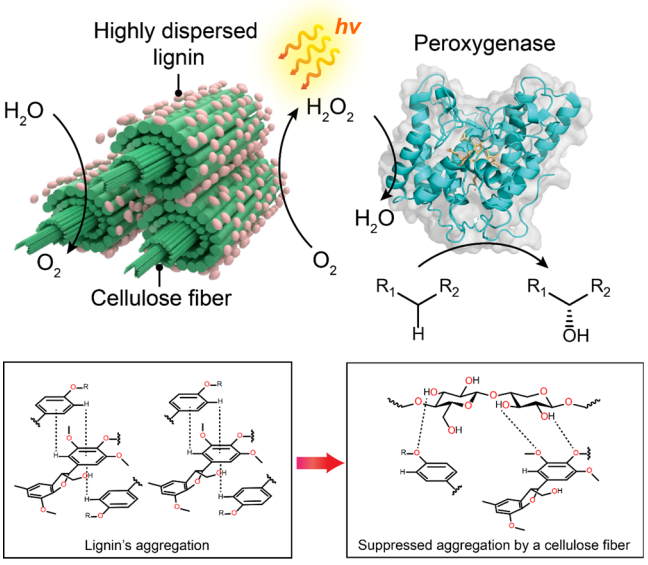

[a]The wood suppresses the self-aggregation of lignin by the lignin-cellulose hydrogen bonding, resulting in uniformly distributed lignins. The highly dispersed lignins on the wood drive a photoreduction of O_2 to H_2O_2, gaining electrons from H_2O. The lignin-driven photoredox reactions are combined with peroxygenase to achieve enantiospecific oxygenation of alkane, benzylic, and styrene compounds.

complete dissolution of lignin and cellulose in ionic liquids, followed by reconstitution in distilled water. The fabricated artificial wood is characterized and compared to lignin by using Fourier transform infrared (FTIR), dynamic light scattering (DLS) analysis, nuclear magnetic resonance (NMR), UV−visible, and photoluminescence (PL) spectroscopies. The lignin within the artificial wood particles is arranged uniformly on cellulose fibers by suppressing self-aggregation through the intermolecular hydrogen bonds between the two components. Thus, it enables lignin to function as a photocatalyst without loss of activity even at high concentrations in reaction media.

Our artificial wood photocatalyst is further combined with unspecific peroxygenase (EC 1.11.2.1) from *Agrocybe aegerita* (*Aae*UPO) to accomplish the oxyfunctionalization of hydrocarbons, which produces numerous value-added compounds for pharmaceutical, bulk, and fine chemical industries. *Aae*UPO is an ideal and green biocatalyst to catalyze the selective oxygenation of inert C−H bonds using H_2O_2 under mild conditions,[14−16] whereas traditional metal catalysts require toxic oxidants and harsh conditions.[17] However, UPOs suffer from the oxidative inactivation of their heme active sites at elevated concentrations of H_2O_2, which can be addressed by in situ H_2O_2 supply.

In this study, with the highly efficient in situ H_2O_2 generation by the artificial wood, *Aae*UPO demonstrates universal biosyntheses of enantiopure alcohols and epoxides by inserting an oxygen atom selectively in the inert C−H bonds in simple organic compounds. This biocatalyst coupled with the artificial wood achieves higher total turnover numbers (TTNs) and turnover frequencies (TOFs) for oxyfunctionalization than that with lignin. The artificial wood photocatalyst provides a new design protocol for maximizing the photoredox ability of lignin and marks a significant milestone in sustainable photobiocatalysis using only solar energy and water as green resources.

EXPERIMENTAL SECTION

Materials. Kraft lignin (product number: 370959), cellulose (medium fibers from softwood pulp), and all the other chemicals were purchased from Sigma-Aldrich (St. Louis, MO, USA) and used without further purification. Recombinant unspecific peroxygenase from *A. aegerita* (r*Aae*UPO) was prepared following the previous work.[18]

Preparation of Artificial Wood Powder. The artificial wood powder was fabricated using a modified method based on our previous work.[19] To 1-ethyl-3-methylimidazolium acetate (5 g) was added lignin (50 mg) and cellulose (50 mg). The solution was then stirred on a magnetic plate under 70 °C for 3 h to obtain a homogeneous mixture. After washing the mixture with deionized water (10 mL) three times, the insoluble powder was precipitated and then separated by centrifugation (8000 rpm, 10 min). After that, the precipitate was vacuum-dried at 55 °C for 12 h to yield artificial wood powder (36.1 mg).

NMR Spectroscopy. $^1H-^{13}C$ heteronuclear single quantum coherence (HSQC) NMR spectra of lignin were acquired employing a 500 MHz AVANCE NEO NMR spectrometer (Bruker, Rheinstetten, Germany) with HSQC pulse sequence (hsqcedetgpsisp 2.3) and parameters according to the literature.[4] Prior to the test, 1 mL of dimethyl sulfoxide (DMSO)-d_6 solution containing the lignin (84 mg mL^{-1}) was put in an NMR tube. The probed $^1H-^{13}C$ cross-peaks were calibrated with the DMSO-d_6 peak (δ_H = 2.5 ppm, δ_C = 39.5 ppm). ^1H solid-state magic angle spinning (MAS) NMR spectra of lignin, cellulose, and artificial wood were obtained by using a Varian VNMRS 600 MHz Solid system (Palo Alto, CA, USA) equipped with a triple-resonance 1.2 mm MAS probe. A 90° ^1H pulse of 1.2 μs was used for a single pulse to enhance the resolution of the ^1H resonance. The ^1H chemical shifts of the samples were calibrated with adamantane.

Estimation of Lignin Loading on the Artificial Wood. To check the amount of lignin present in the artificial wood, lignin was extracted from the wood powder by using DMSO until the supernatant became transparent. The lignin content was obtained by subtracting the weight after extraction from that of the wood before extraction. The process was repeated three times with the artificial wood samples and then averaged to estimate the lignin loading on the wood.

Photobiocatalytic Oxyfunctionalization and Product Quantification. Photobiocatalytic oxyfunctionalization reactions were performed in the O_2-saturated sodium phosphate (NaPi) buffer (100 mM, pH 7.0) containing r*Aae*UPO (250 nM), a substrate (40 mM), such as ethylbenzene, tetralin, cis-β-methylstyrene, and 2,3-dimethylbutane, with the lignin or artificial wood at a desired concentration. During the reaction, the reaction medium was illuminated with a xenon lamp (I = 100 mW cm^{-2}, 260 nm < λ < 900 nm). The oxyfunctionalized products were extracted with an ethyl acetate solution containing 1-octanol (5 mM, internal standard) and were quantified by a 7890A gas chromatograph (Agilent) equipped

https://doi.org/10.1021/acssuschemeng.4c02882
ACS Sustainable Chem. Eng. 2024, 12, 8950−8957

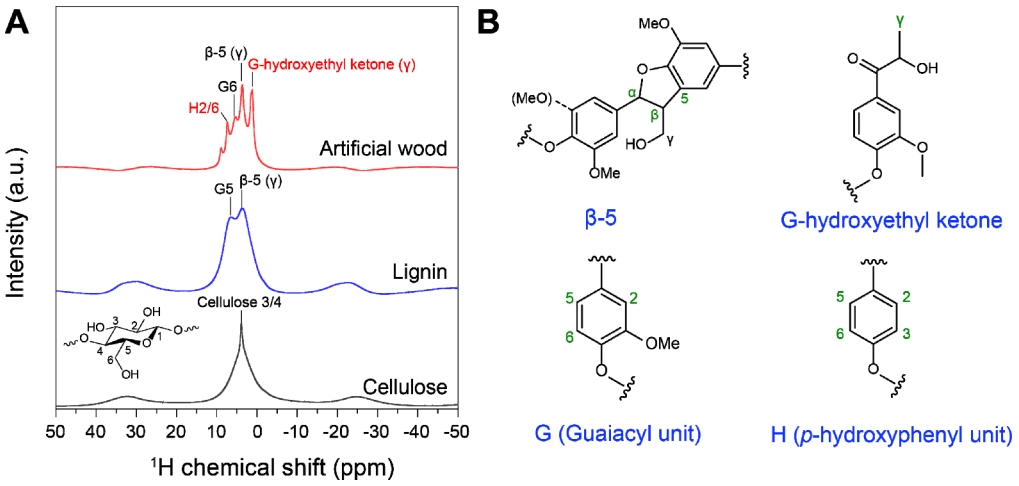

Figure 1. (A) ^{1}H solid-state NMR spectra of artificial wood, lignin, and cellulose. The inset indicates the structure of cellulose. (B) Structural motifs in the lignins, probed in ^{1}H solid-state NMR experiments. Phenylcoumaran (β-5), G-hydroxyethyl ketone, guaiacyl unit (G), and *p*-hydroxyphenyl unit (H). The characters of α, β, γ, 2, 3, 5, and 6 indicate the specific carbons of lignin's unit.

with the CP chirasil-Dex CB column and a flame ionization detector. The analytical conditions were the same as described in our previous study.[20] The TTN, TOF, and enantiomeric excess (ee) were evaluated following the eqs 1−3:

$$\text{TTN} = \frac{\text{Maximum product (mM) at a given time}}{\text{r}\textit{Aae}\text{UPO(mM)}} \quad (1)$$

$$\text{TOF (min}^{-1}\text{)} = \frac{\text{Product (mM)}}{\text{r}\textit{Aae}\text{UPO (mM)} \times \text{reaction time (min)}} \quad (2)$$

$$\text{ee (\%)} = \frac{R \text{ form (mol)} - S \text{ form (mol)}}{\text{Total products (mol)}} \times 100\% \quad (3)$$

RESULTS AND DISCUSSION

Solid-State Characterization of Artificial Wood Particles. To understand the self-aggregation of lignin at a molecular level, we examined the chemical structure of lignin using ^{1}H−^{13}C heteronuclear single quantum coherence (HSQC) NMR spectroscopy. Kraft lignin was used because it was found to have optimum photocatalytic properties for O_2 reduction, such as strong light absorption and slow charge recombination among various lignins (lignosulfonate, cellulolytic enzyme lignin, and lignin dehydrogenation polymer).[4] In the 2D NMR spectra, the lignin showed ^{1}H−^{13}C cross-peaks relative to the native units (β-aryl ether (β-O-4), phenylcoumaran (β-5), resinol (β−β), guaiacyl propanol, secoisolariciresinol, G, and H units)[21,22] and the kraft-derived units (β-5 stilbene, enol ether, and guaiacyl hydroxyethyl ketone) (Figure S1).[22,23] These aromatic rings and multiple functional groups induce the interactions between lignin molecules.[24,25] For example, the phenyl rings form noncovalent π−π interactions, and the aliphatic hydroxyl, phenolic hydroxyl, and carboxyl groups form hydrogen bonds.[11]

To suppress the self-aggregation of lignin, we have introduced cellulose to form molecular interactions (e.g., hydrogen bonding) with lignin, inspired by woody cell walls. The wood-mimetic particles were prepared by the dissolution of lignin and cellulose fibers in the ionic liquid (1-ethyl-3-methylimidazolium acetate) followed by reconstitution with distilled water (see the Experimental Section). It was found that the fabricated wood particles contained 29 wt % of lignin content and had no residual ionic liquid (Figure S2). Whether cellulose can prevent lignin aggregation was investigated using ^{1}H NMR, FTIR analysis, and UV−visible spectroscopy as a solid state. For comparison, lignin was also examined under the same conditions.

First, we conducted ^{1}H solid-state magic angle spinning NMR analysis to compare the physicochemical states of the lignin and artificial wood powders. Compared to solution ^{1}H−^{13}C HSQC NMR results (Figure S1), the pristine lignin displayed only two resonances of β-5 (3.7 ppm) and the G unit (6.8 ppm) (Figure 1a,b). The severe aggregation in the pristine lignin impeded the NMR sensitivity,[26−28] leading to the diminished peak intensity of β-O-4, β−β, β-5 stilbene, enol ether, and H units, which were observed in the dissolved lignin. In contrast, the artificial wood revealed resonances of guaiacyl hydroxyethyl ketone (1.3 ppm) and the H unit (7.4 ppm) in addition to the β-5 and G units, indicating the suppressed aggregation. The intermolecular interactions (e.g., hydrogen bonding) between the lignin and cellulose in the wood are believed to restrain the self-aggregation behavior of the lignin (Scheme 1). The disappearance of cellulose's X-ray diffraction pattern in the artificial wood also corroborates specific interactions, which reduce the crystallinity of cellulose fibers (Figure S3).

Building upon the chemical identification of artificial wood, we examined the intermolecular interactions between lignin and cellulose in artificial wood using FTIR analysis. The characteristic peaks of C=C stretching in lignin were red-shifted (~25 cm^{-1}) after coupling with cellulose in the wood, indicative of restrained π−π stacking of lignin (weakening of C=C bond)[29,30] by lignin-cellulose interactions (Figure S4a). The peaks of hydroxyl and ether groups in the lignin were also red-shifted with cellulose, related to the hydrogen bonding between the lignin and cellulose (Figure S4).[31,32] These results denote that the interactions between the lignin and cellulose in the artificial wood can impede lignin aggregation.[27]

To further investigate the effect of cellulose on suppressing the self-aggregation of lignin, we identified IR imaging of the lignin and wood samples. The lignin displayed the massive intensity variation of C=C (aromatic compound), C−O (ether), and O−H (alcohol) bonds, representing the heavy aggregation by the strong electrostatic forces (i.e., π−π

https://doi.org/10.1021/acssuschemeng.4c02882
ACS Sustainable Chem. Eng. 2024, 12, 8950−8957

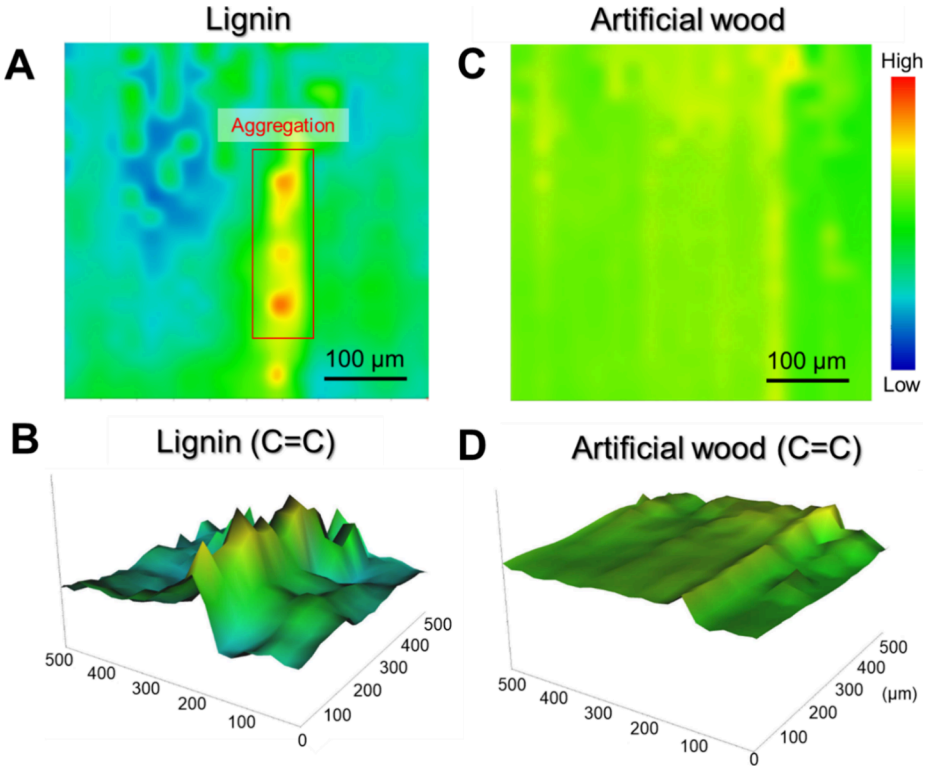

Figure 2. (A) FTIR spectroscopic imaging of lignin and (B) corresponding intensity profiles of the ν(C═C) band. The red box region indicates high intensity of the ν(C═C) band, originating from $\pi-\pi$ aggregation of the lignin. (C) FTIR spectroscopic imaging of artificial wood and (D) corresponding intensity profiles of the ν(C═C) band. Sample area: 500 μm × 500 μm.

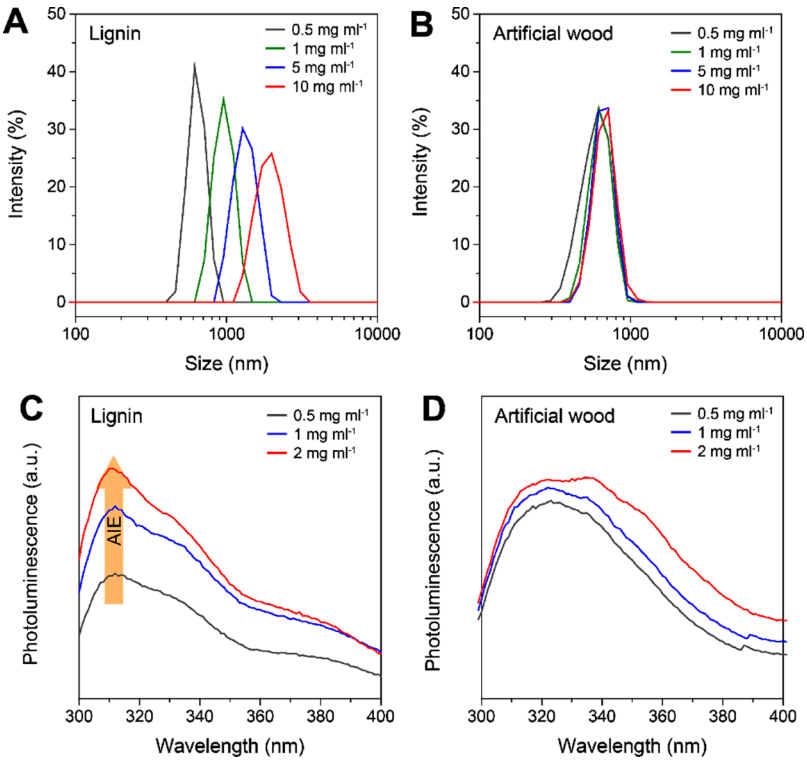

Figure 3. Size distribution of (A) dispersed lignin and (B) artificial wood obtained from DLS measurements. Electrolyte: NaPi buffer (100 mM, pH 7.0). PL spectra of (C) lignin and (D) artificial wood. AIE: aggregation-induced emission. Excitation: 280 nm.

stacking and hydrogen bonding) between lignin molecules (Figures 2a,b, S5, and S6). On the contrary, the artificial wood manifested a uniform distribution of the functional groups with negligible intensity variation, pointing to a homogeneous spatial arrangement of lignin on the cellulose fibers (Figures 2c,d, S5, and S6). Benefiting from the highly dispersed lignin in

https://doi.org/10.1021/acssuschemeng.4c02882
ACS Sustainable Chem. Eng. 2024, 12, 8950−8957

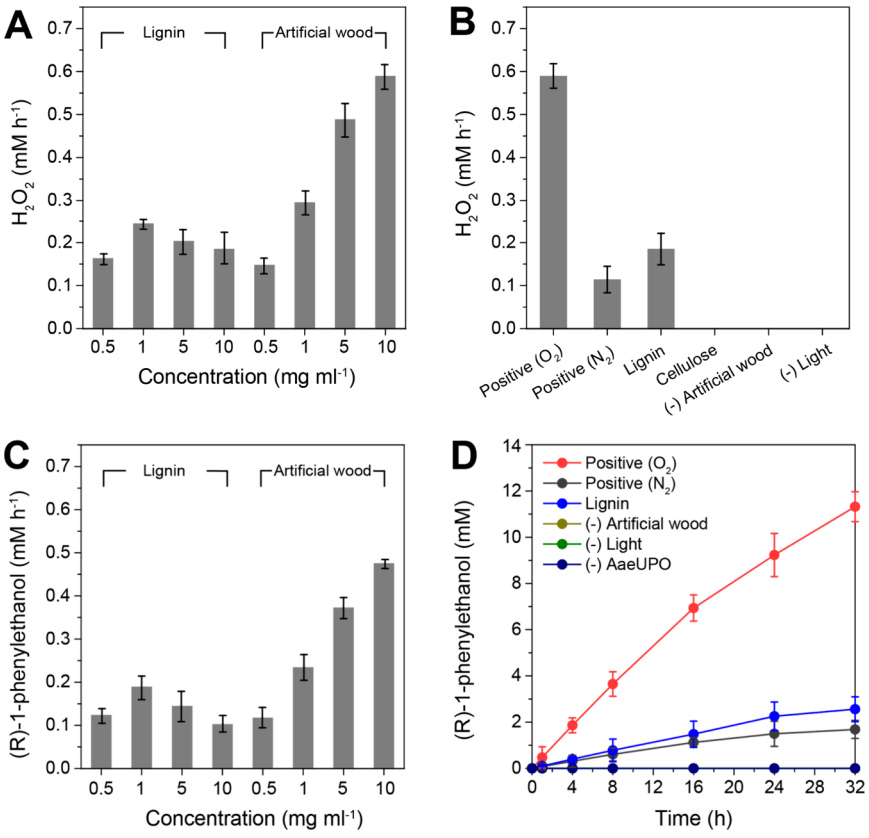

Figure 4. (A) Production rate of H_2O_2 with different concentrations of lignin and artificial wood. (B) Control experiments on a H_2O_2 generation by artificial wood. (C) Production rate of (*R*)-1-phenylethanol with different concentrations of lignin and artificial wood. (D) Time profile of the photobiocatalytic oxyfunctionalization of ethylbenzene to (*R*)-1-phenylethanol with artificial wood. Light source: xenon (I = 100 mW cm^{-2}, 260 nm < λ < 900 nm). Electrolyte: O_2-saturated NaPi buffer (100 mM, pH 7.0) containing artificial wood (10 mg mL^{-1}).

the artificial wood, it showed stronger absorption of UV and visible light compared to its lignin counterpart (Figure S7).

Characterization of Artificial Wood Particles in Solution. We also examined the artificial wood particles in a NaPi buffer (100 mM, pH 7.0) using DLS analysis and PL spectroscopy. As the concentration was increased from 0.5 to 10 mg mL^{-1}, the lignin agglomerated and increased in size, whereas the wood showed an insignificant change. Thus, the artificial wood particles were on average 2.7 times smaller than the lignin at a high concentration of 10 mg mL^{-1} (Figure 3a,b). In addition, the wood strikingly reduced the aggregation-induced emission of the lignin with increasing concentration (up to 2 mg mL^{-1}), reconfirming the restraint of aggregation (Figures 3c,d and S8).[24,33,34] All of the analysis results clearly demonstrate that the self-aggregation of lignin is suppressed by cellulose fibers in the artificial wood.

Photocatalytic H_2O_2 Generation by Artificial Wood and Enantioselective Photobiocatalytic Oxyfunctionalization. We checked the photoredox ability of the artificial wood for H_2O_2 generation under solar irradiation (I: 100 mW cm^{-2}, λ: 260 to 900 nm) for 120 min. The wood produced both the H_2O_2 (1.12 mM) and O_2 (0.483 mM) simultaneously (Figure S9), which is attributed to the lignin's photoredox power to trigger O_2 reduction to H_2O_2 (the reduction potential, E_{red} = 0.68 V versus RHE (reversible hydrogen electrode)) and H_2O oxidation to O_2 (the oxidation potential, E_{ox} = 1.23 V vs RHE). The LUMO (lowest-unoccupied molecular orbital) level of kraft lignin (−0.24 V vs RHE) is more negative than E_{red}, and the HOMO (highest-occupied molecular orbital) level (2.69 V vs RHE) is more positive than E_{ox}.[4] To highlight the merits of our system, we conducted the photoreduction of O_2 to H_2O_2 while increasing the concentration of the photocatalysts (i.e., lignin and artificial wood powders). Generally, using high concentrations of photocatalysts is a facile strategy to augment the productivity of photoredox reactions.[35−37] However, the lignin manifested a decreased H_2O_2 production as the concentration increased from 1 to 10 mg mL^{-1} (Figure 4a). This may be due to the decrease and/or quenching of redox sites, resulting from the higher degree of aggregation with increased concentrations of lignin.[5−9] By contrast, the H_2O_2 production rate of the wood continued to increase to 0.59 mM h^{-1} at 10 mg mL^{-1} due to the suppressed aggregation of lignin in the wood. Control tests in the absence of O_2, lignin, and light led to insignificant H_2O_2 generations, corroborating that H_2O_2 was produced from the photoreduction of O_2 by lignin (Figure 4b).

Next, we coupled the photocatalytic system with r*Aae*UPO biocatalysis to yield value-added oxygenation products. The intensified oxidative fluorescence quenching of the artificial wood with O_2, r*Aae*UPO, and ethylbenzene indicated the successful cascade of light-induced electron transfer from the wood to ethylbenzene via O_2 and r*Aae*UPO for oxyfunctionalization (Figure S10). For the photobiocatalytic oxygenation of ethylbenzene to (*R*)-1-phenylethanol, the wood yielded a 4.4 times higher concentration of the product (11.3 mM at 10 mg mL^{-1} for 32 h reaction) compared to the lignin, showing the superiority as a photocatalyst (Figure 4c,d). We further demonstrated the universal applicability of the

https://doi.org/10.1021/acssuschemeng.4c02882
ACS Sustainable Chem. Eng. 2024, 12, 8950−8957

artificial wood by expanding the substrate scope of r*Aae*UPO. The wood-r*Aae*UPO hybrid system produced various invaluable products, which are applied to pharmaceutical industries,[38,39] by catalyzing the hydroxylation of ethylbenzene (TTN: 45,300 and TOF: 31.6 min^{-1}), tetralin (35,600 and 25.8 min^{-1}), and 2,3-dimethylbutane (30,000 and 21.4 min^{-1}) and the epoxidation of *cis*-*β*-methylstyrene (16,500 and 11.7 min^{-1}) with high selectivity (>99%) (Figure 5a,b). The

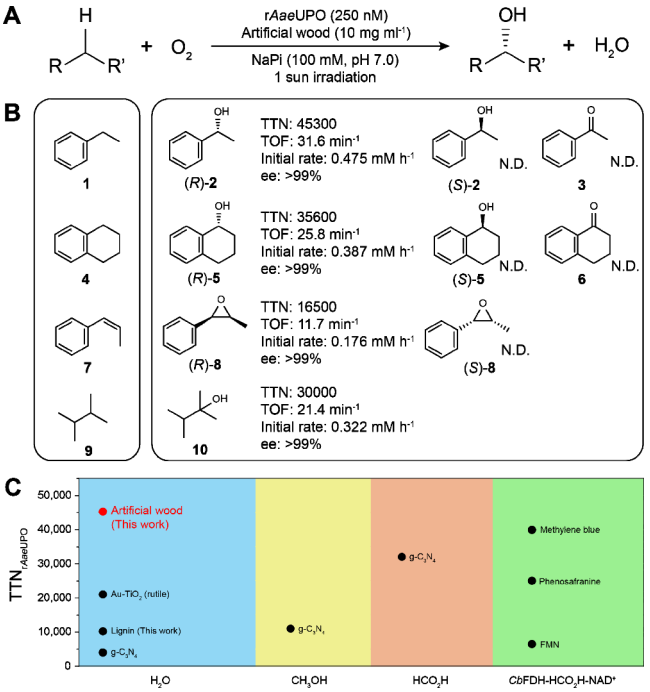

Figure 5. (A) Reaction equation of the photobiocatalytic oxyfunctionalization of hydrocarbon substrates by the r*Aae*UPO and artificial wood. (B) Substrate scope of photobiocatalytic oxyfunctionalization using ethylbenzene (**1**), tetralin (**4**), *cis*-*β*-methylstyrene (**7**), and 2,3-dimethylbutane (**9**). Main products: *R*-forms of 1-phenylethanol (**2**), 1,2,3,4-tetrahydro-1-naphthol (**5**), 2-methyl-3-phenyloxirane (**8**), and 2,3-dimethylbutan-2-ol (**10**). Possible byproducts: acetophenone (**3**) and *α*-tetralone (**6**). TTN and TOF were calculated at reaction times of 32 and 1 h, respectively. Electrolyte: O_2-saturated NaPi buffer (100 mM, pH 7.0) containing artificial wood (10 mg mL^{-1}) and r*Aae*UPO (250 nM). Light source: xenon lamp, 1 sun. (C) TTN comparison of relevant r*Aae*UPO-driven ethylbenzene hydroxylation using photocatalysts.[4,20,40−44]

catalytic turnover of artificial wood-r*Aae*UPO outperformed that of lignin-r*Aae*UPO shown in Figure S11 and was also compared to those of other systems reported in the literature (Figure 5c). Most photocatalysts (e.g., methylene blue, phenosafranine, flavin mononucleotide, and graphitic C_3N_4) showed the TTNs (<40,000) for ethylbenzene hydroxylation despite the use of costly electron donors, not water.[40−44]

CONCLUSIONS

For the first time, we present an artificial wood photocatalyst for practical solar-driven oxygenation biosynthesis. Lignin, a major waste in the pulp and biorefinery industry, has recently been identified as a sustainable photocatalyst. Although the aromatic and hydroxyl groups endow lignin with a photocatalytic activity for H_2O_2 production from O_2, their propensity to form aggregation screens the redox sites of lignin, limiting the practical applications of a lignin photocatalyst, particularly at high concentrations. Introduction of cellulose to mimic woody cell walls suppressed its aggregation by intermolecular hydrogen bonding between lignin and cellulose. As a result, the artificial wood exhibited a 3.2 times higher H_2O_2 generation rate than lignin at a high concentration of 10 mg mL^{-1}. Furthermore, the wood-mimetic photocatalyst was coupled with r*Aae*UPO biocatalyst, and this hybrid catalyst realized a universal solar-driven oxygenation reaction for various value-added chemicals with higher TTNs and TOFs than those of the lignin hybrid catalyst. This work suggests a practical strategy to utilize waste lignin as a photocatalyst and demonstrates sustainable bio-oxygenation reactions using sunlight and water as energy and electron sources, respectively.

ASSOCIATED CONTENT

Data Availability Statement

The data underlying this study are available in the published article and its Supporting Information.

Supporting Information

The Supporting Information is available free of charge at https://pubs.acs.org/doi/10.1021/acssuschemeng.4c02882.

Experimental details for material charaterization and H_2O_2 and O_2 quantification, HSQC NMR spectra of lignin, X-ray diffraction, FTIR, absorbance, H_2O_2/O_2 production, and PL data of artificial wood, and experimental results on photobiocatalytic oxyfunctionalization of hydrocarbon substrates by lignin and UPO (PDF)

AUTHOR INFORMATION

Corresponding Authors

Keehoon Won − *Department of Chemical and Biochemical Engineering, Dongguk University-Seoul, Seoul 04620, Republic of Korea;* orcid.org/0000-0002-0763-7683; Email: keehoon@dongguk.edu

Chan Beum Park − *Department of Materials Science and Engineering, Korea Advanced Institute of Science and Technology, Daejeon 34141, Republic of Korea;* orcid.org/0000-0002-0767-8629; Email: parkcb@kaist.ac.kr

Authors

Jinha Jang − *Department of Materials Science and Engineering, Korea Advanced Institute of Science and Technology, Daejeon 34141, Republic of Korea*

Waseela Aurangzeb Khan − *Department of Materials Science and Engineering, Korea Advanced Institute of Science and Technology, Daejeon 34141, Republic of Korea*

Frank Hollmann − *Department of Biotechnology, Delft University of Technology, 2629HZ Delft, The Netherlands;* orcid.org/0000-0003-4821-756X

Complete contact information is available at: https://pubs.acs.org/10.1021/acssuschemeng.4c02882

Notes

The authors declare no competing financial interest.

ACKNOWLEDGMENTS

This work was supported by the National Research Foundation of Korea (grant numbers: NRF-

2015R1A3A2066191 and RS-2023-00222078), Republic of Korea.

REFERENCES

(1) Wang, D.; Lee, S. H.; Kim, J.; Park, C. B. Waste to Wealth": Lignin as a renewable building block for energy harvesting/storage and environmental remediation. *ChemSusChem* **2020**, *13* (11), 2807−2827.
(2) Yu, X.; Yang, B.; Zhu, W.; Deng, T.; Pu, Y.; Ragauskas, A.; Wang, H. Towards functionalized lignin and its derivatives for high-value material applications. *Ind. Crops Prod.* **2023**, *200*, No. 116824.
(3) Chatel, G.; Rogers, R. D. Review: Oxidation of lignin using ionic liquids—an innovative strategy to produce renewable chemicals. *ACS Sustain. Chem. Eng.* **2014**, *2* (3), 322−339.
(4) Kim, J.; Nguyen, T. V. T.; Kim, Y. H.; Hollmann, F.; Park, C. B. Lignin as a multifunctional photocatalyst for solar-powered biocatalytic oxyfunctionalization of C−H bonds. *Nat. Synth.* **2022**, *1* (3), 217−226.
(5) Daďová, J.; Kümmel, S.; Feldmeier, C.; Cibulková, J.; Pažout, R.; Maixner, J.; Gschwind, R. M.; König, B.; Cibulka, R. Aggregation effects in visible-light flavin photocatalysts: synthesis, structure, and catalytic activity of 10-arylflavins. *Chem.—Eur. J.* **2013**, *19* (3), 1066−1075.
(6) Iliev, V.; Alexiev, V.; Bilyarska, L. Effect of metal phthalocyanine complex aggregation on the catalytic and photocatalytic oxidation of sulfur containing compounds. *J. Mol. Catal. A Chem.* **1999**, *137* (1), 15−22.
(7) Ren, S.; Lees, E. W.; Hunt, C.; Jewlal, A.; Kim, Y.; Zhang, Z.; Mowbray, B. A. W.; Fink, A. G.; Melo, L.; Grant, E. R.; et al. Catalyst aggregation matters for immobilized molecular CO_2RR electrocatalysts. *J. Am. Chem. Soc.* **2023**, *145* (8), 4414−4420.
(8) Chen, X.; Hu, X.-M.; Daasbjerg, K.; Ahlquist, M. S. G. Understanding the enhanced catalytic CO_2 reduction upon adhering cobalt porphyrin to carbon nanotubes and the inverse loading effect. *Organometallics.* **2020**, *39* (9), 1634−1641.
(9) Gerdes, R.; Wöhrle, D.; Spiller, W.; Schneider, G.; Schnurpfeil, G.; Schulz-Ekloff, G. Photo-oxidation of phenol and monochlorophenols in oxygen-saturated aqueous solutions by different photosensitizers. *J. Photochem. Photobiol., A* **1997**, *111* (1), 65−74.
(10) Contreras, S.; Gaspar, A. R.; Guerra, A.; Lucia, L. A.; Argyropoulos, D. S. Propensity of lignin to associate: light scattering photometry study with native lignins. *Biomacromolecules* **2008**, *9* (12), 3362−3369.
(11) Zhao, W.; Xiao, L.-P.; Song, G.; Sun, R.-C.; He, L.; Singh, S.; Simmons, B. A.; Cheng, G. From lignin subunits to aggregates: insights into lignin solubilization. *Green Chem.* **2017**, *19* (14), 3272−3281.
(12) Atalla, R. H.; Agarwal, U. P. Raman microprobe evidence for lignin orientation in the cell walls of native woody tissue. *Science* **1985**, *227* (4687), 636−638.
(13) Agarwal, U. P.; Atalla, R. H. In-situ Raman microprobe studies of plant cell walls: Macromolecular organization and compositional variability in the secondary wall of Picea mariana (Mill.) B.S.P. *Planta* **1986**, *169* (3), 325−332.
(14) Yun, C.-H.; Kim, J.; Hollmann, F.; Park, C. B. Light-driven biocatalytic oxidation. *Chem. Sci.* **2022**, *13* (42), 12260−12279.
(15) Bordeaux, M.; Galarneau, A.; Drone, J. Catalytic, mild, and selective oxyfunctionalization of linear alkanes: current challenges. *Angew. Chem., Int. Ed.* **2012**, *51* (43), 10712−10723.
(16) Hofrichter, M.; Ullrich, R. Oxidations catalyzed by fungal peroxygenases. *Curr. Opin. Chem. Biol.* **2014**, *19*, 116−125.
(17) Enthaler, S.; Company, A. Palladium-catalysed hydroxylation and alkoxylation. *Chem. Soc. Rev.* **2011**, *40* (10), 4912−4924.
(18) Molina-Espeja, P.; Ma, S.; Mate, D. M.; Ludwig, R.; Alcalde, M. Tandem-yeast expression system for engineering and producing unspecific peroxygenase. *Enzyme Microb. Technol.* **2015**, *73*−*74*, 29−33.
(19) Lee, M.; Kim, J. H.; Lee, S. H.; Lee, S. H.; Park, C. B. Biomimetic artificial photosynthesis by light-harvesting synthetic wood. *ChemSusChem* **2011**, *4* (5), 581−586.
(20) Lee, C. H.; Kim, J.; Park, C. B. Z-Schematic artificial leaf structure for biosolar oxyfunctionalization of hydrocarbons. *ACS Energy Lett.* **2023**, *8* (6), 2513−2521.
(21) Sáez-Jiménez, V.; Rencoret, J.; Rodríguez-Carvajal, M. A.; Gutiérrez, A.; Ruiz-Dueñas, F. J.; Martínez, A. T. Role of surface tryptophan for peroxidase oxidation of nonphenolic lignin. *Biotechnol. Biofuels* **2016**, *9* (1), 198.
(22) Lancefield, C. S.; Wienk, H. L. J.; Boelens, R.; Weckhuysen, B. M.; Bruijnincx, P. C. A. Identification of a diagnostic structural motif reveals a new reaction intermediate and condensation pathway in kraft lignin formation. *Chem. Sci.* **2018**, *9* (30), 6348−6360.
(23) Crestini, C.; Lange, H.; Sette, M.; Argyropoulos, D. S. On the structure of softwood kraft lignin. *Green Chem.* **2017**, *19* (17), 4104−4121.
(24) Deng, Y.; Feng, X.; Zhou, M.; Qian, Y.; Yu, H.; Qiu, X. Investigation of aggregation and assembly of alkali lignin using iodine as a probe. *Biomacromolecules* **2011**, *12* (4), 1116−1125.
(25) Jawerth, M. E.; Brett, C. J.; Terrier, C.; Larsson, P. T.; Lawoko, M.; Roth, S. V.; Lundmark, S.; Johansson, M. Mechanical and morphological properties of lignin-based thermosets. *ACS Appl. Polym. Mater.* **2020**, *2* (2), 668−676.
(26) Märker, K.; Paul, S.; Fernández-de-Alba, C.; Lee, D.; Mouesca, J.-M.; Hediger, S.; De Paëpe, G. Welcoming natural isotopic abundance in solid-state NMR: probing π-stacking and supramolecular structure of organic nanoassemblies using DNP. *Chem. Sci.* **2017**, *8* (2), 974−987.
(27) Kang, X.; Kirui, A.; Dickwella Widanage, M. C.; Mentink-Vigier, F.; Cosgrove, D. J.; Wang, T. Lignin-polysaccharide interactions in plant secondary cell walls revealed by solid-state NMR. *Nat. Commun.* **2019**, *10* (1), 347.
(28) Jang, J.; Shin, J.-S.; Ko, S.; Park, H.; Song, W.-J.; Park, C. B.; Kang, J. Self-assembled protective layer by symmetric ionic liquid for long-cycling lithium−metal batteries. *Adv. Energy Mater.* **2022**, *12* (13), No. 2103955.
(29) Vasylyeva, V.; Catalano, L.; Nervi, C.; Gobetto, R.; Metrangolo, P.; Resnati, G. Characteristic redshift and intensity enhancement as far-IR fingerprints of the halogen bond involving aromatic donors. *CrystEngComm.* **2016**, *18* (13), 2247−2250.
(30) Notley, S. M.; Norgren, M. Surface energy and wettability of spin-coated thin films of lignin isolated from wood. *Langmuir* **2010**, *26* (8), 5484−5490.
(31) Zhang, Y.; Haque, A. N. M. A.; Naebe, M. UV-functional flexible nanocomposite film with high lignin-cellulose nanocrystals content. *J. Mater. Res. Technol.* **2023**, *26*, 5990−6000.
(32) Hambardzumyan, A.; Foulon, L.; Chabbert, B.; Aguié-Béghin, V. Natural organic UV-absorbent coatings based on cellulose and lignin: designed effects on spectroscopic properties. *Biomacromolecules* **2012**, *13* (12), 4081−4088.
(33) Ma, Z.; Liu, C.; Niu, N.; Chen, Z.; Li, S.; Liu, S.; Li, J. Seeking brightness from nature: J-aggregation-induced emission in cellulolytic enzyme lignin nanoparticles. *ACS Sustain. Chem. Eng.* **2018**, *6* (3), 3169−3175.
(34) Xue, Y.; Qiu, X.; Ouyang, X. Insights into the effect of aggregation on lignin fluorescence and its application for microstructure analysis. *Int. J. Biol. Macromol.* **2020**, *154*, 981−988.
(35) Lee, S. H.; Choi, D. S.; Pesic, M.; Lee, Y. W.; Paul, C. E.; Hollmann, F.; Park, C. B. Cofactor-Free, direct photoactivation of enoate reductases for the asymmetric reduction of C = C Bonds. *Angew. Chem., Int. Ed.* **2017**, *56* (30), 8681−8685.
(36) Fan, Y.; Zhou, W.; Qiu, X.; Li, H.; Jiang, Y.; Sun, Z.; Han, D.; Niu, L.; Tang, Z. Selective photocatalytic oxidation of methane by quantum-sized bismuth vanadate. *Nat. Sustain.* **2021**, *4* (6), 509−515.
(37) Kuk, S. K.; Jang, J.; Kim, J.; Lee, Y.; Kim, Y. S.; Koo, B.; Lee, Y. W.; Ko, J. W.; Shin, B.; Lee, J.-K.; Park, C. B. CO_2-Reductive, copper oxide-based photobiocathode for Z-Scheme semi-artificial leaf structure. *ChemSusChem* **2020**, *13* (11), 2940−2944.

https://doi.org/10.1021/acssuschemeng.4c02882
ACS Sustainable Chem. Eng. 2024, 12, 8950−8957

(38) Yoon, J.; Jang, H.; Oh, M.-W.; Hilberath, T.; Hollmann, F.; Jung, Y. S.; Park, C. B. Heat-fueled enzymatic cascade for selective oxyfunctionalization of hydrocarbons. *Nat. Commun.* **2022**, *13* (1), 3741.
(39) Lee, S. H.; Choi, D. S.; Kuk, S. K.; Park, C. B. Photobiocatalysis: activating redox enzymes by direct or indirect transfer of photoinduced electrons. *Angew. Chem., Int. Ed.* **2018**, *57* (27), 7958−7985.
(40) Choi, D. S.; Lee, H.; Tieves, F.; Lee, Y. W.; Son, E. J.; Zhang, W.; Shin, B.; Hollmann, F.; Park, C. B. Bias-free in situ H_2O_2 generation in a photovoltaic-photoelectrochemical tandem cell for biocatalytic oxyfunctionalization. *ACS Catal.* **2019**, *9* (11), 10562−10566.
(41) Zhang, W.; Fernández-Fueyo, E.; Ni, Y.; van Schie, M.; Gacs, J.; Renirie, R.; Wever, R.; Mutti, F. G.; Rother, D.; Alcalde, M.; Hollmann, F. Selective aerobic oxidation reactions using a combination of photocatalytic water oxidation and enzymatic oxyfunctionalizations. *Nat. Catal.* **2018**, *1* (1), 55−62.
(42) Zhang, W.; Burek, B. O.; Fernández-Fueyo, E.; Alcalde, M.; Bloh, J. Z.; Hollmann, F. Selective activation of C−H Bonds in a cascade process combining photochemistry and biocatalysis. *Angew. Chem., Int. Ed.* **2017**, *56* (48), 15451−15455.
(43) van Schie, M. M. C. H.; Zhang, W.; Tieves, F.; Choi, D. S.; Park, C. B.; Burek, B. O.; Bloh, J. Z.; Arends, I. W. C. E.; Paul, C. E.; Alcalde, M.; Hollmann, F. Cascading g-C_3N_4 and peroxygenases for selective oxyfunctionalization reactions. *ACS Catal.* **2019**, *9* (8), 7409−7417.
(44) Willot, S. J. P.; Fernández-Fueyo, E.; Tieves, F.; Pesic, M.; Alcalde, M.; Arends, I. W. C. E.; Park, C. B.; Hollmann, F. Expanding the spectrum of light-driven peroxygenase reactions. *ACS Catal.* **2019**, *9* (2), 890−894.

https://doi.org/10.1021/acssuschemeng.4c02882
ACS Sustainable Chem. Eng. 2024, 12, 8950−8957